ACS OMEGA

Open Access

http://pubs.acs.org/journal/acsodf

Article

Phytoconstituents of *Hericium erinaceus* Exert Benefits for ADHD Conditions by Targeting SLC6A4: Extraction, Spectroscopic Characterization, Phytochemical Screening, *In Vitro*, and Computational Perspectives

Kamalaharshini Mohan, Nandhakumar Ravichandran, Harish Rajendran, Jency Roshni, Mahema Sivakumar, Janakiraman Velayudam, Sheikh F. Ahmad, Haneen A. Al-Mazroua, and Shiek SSJ Ahmed*

Cite This: *ACS Omega* 2025, 10, 4261−4275

Read Online

ACCESS | Metrics & More | Article Recommendations | Supporting Information

ABSTRACT: Attention-deficit/hyperactivity disorder (ADHD) is a persistent neurodevelopmental disorder. Despite pharmacological interventions, there is a need for effective lead molecules and therapeutic targets. Recently, *Hericium erinaceus* (HE) has been traditionally reported to treat various diseases. Herein, we aimed to explore the noncytotoxic properties, phytochemical composition, and spectroscopic characterization of HE aqueous extract. Additionally, we used computational workflows to identify key therapeutic targets for ADHD and assess HE extract phytoconstituents for potential targeting. Initially, the HE aqueous extract was obtained using Soxhlet extraction, and its cytotoxicity was assessed on SH-SY5Y cells using MTT assays. FTIR spectroscopy characterized the extract's functional groups, while biochemical methods and GC−MS identified its phytochemical constituents. A protein−protein interaction network identified ADHD targets, and molecular docking, dynamics, and QM/MM calculations were used to find potential drug candidates from the HE extract. As a result, the HE extract exhibited no cytotoxicity in SH-SY5Y cells across concentrations (0.625 to 10 μg/mL) after 24 h. FTIR spectroscopic analysis detected 13 different functional groups that hold diverse biological importance. Qualitative phytochemical screening revealed the presence of carbohydrates, flavonoids, anthocyanins, tannins, alkaloids, saponins, steroids, and phenolic compounds. GC−MS profiling identified 17 diverse metabolites. Simultaneously, ADHD-related genes and known therapeutic protein targets were integrated into a network, identifying SLC6A4 as a hub target. Molecular docking of HE extract compounds showed myo-inositol's high binding efficiency (−6.53 kcal/mol). Dynamic simulations demonstrated stable interactions, and QM/MM analysis confirmed myo-inositol's ability to transfer electrons, reinforcing its interaction potential. Overall, the HE aqueous extract shows a potent nontoxic profile and contains phytoconstituents like myo-inositol, offering promising therapeutic potential by targeting SLC6A4 for ADHD.

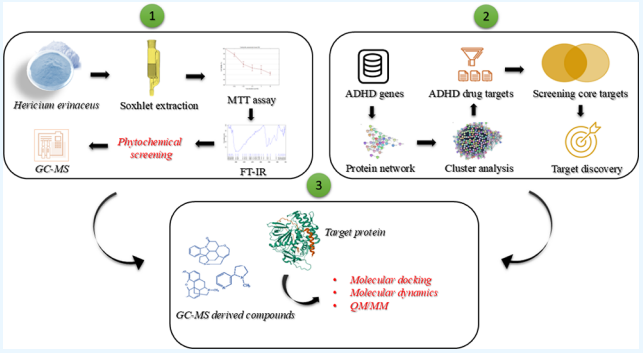

1. INTRODUCTION

Attention deficit hyperactivity disorder (ADHD), a multifactorial neurodevelopmental disorder, is primarily distinguished by inattention, hyperactivity, and impulsiveness.[1] Recently, the worldwide prevalence of ADHD in adults and children was 2.5% and 7.6%, respectively, with symptoms persisting for lifetime in most patients.[2] In addition, ADHD often involves other psychiatric conditions like depression, anxiety, oppositional defiant disorder, academic failures, accidental injury, criminal behavior, and suicide.[3] With its increasing frequency, ADHD has emerged as a significant global health issue.[4] Although dopamine (DA) defects are implicated as core pathogenic factors according to Drechsler et al., 2020, the precise mechanisms remain to be fully elucidated.[5] Currently, methylphenidate (MPH) stands as the most prevalent first-line medication in clinical practice, offering significant short-term relief from ADHD symptoms. MPH blocks the dopamine transporter protein (DAT) and ultimately elevates the availability of extracellular dopamine in the synaptic cleft. Unfortunately, the MPH stimulant carries

Received: June 13, 2024
Revised: January 13, 2025
Accepted: January 22, 2025
Published: January 31, 2025

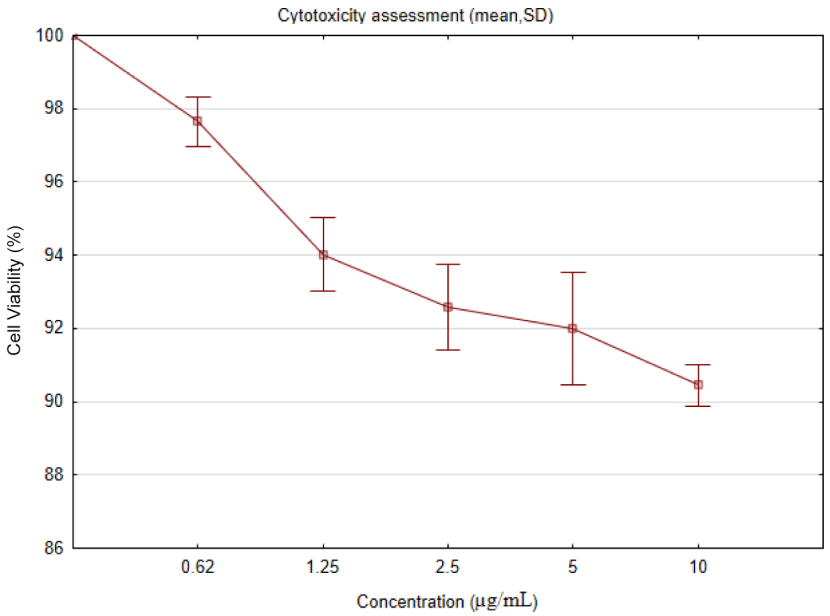

Figure 1. Percentage of SH-SY5Y cell viability post-*Hericium erinaceus* treatment at concentrations ranging from 0.625 to 10 μg/mL.

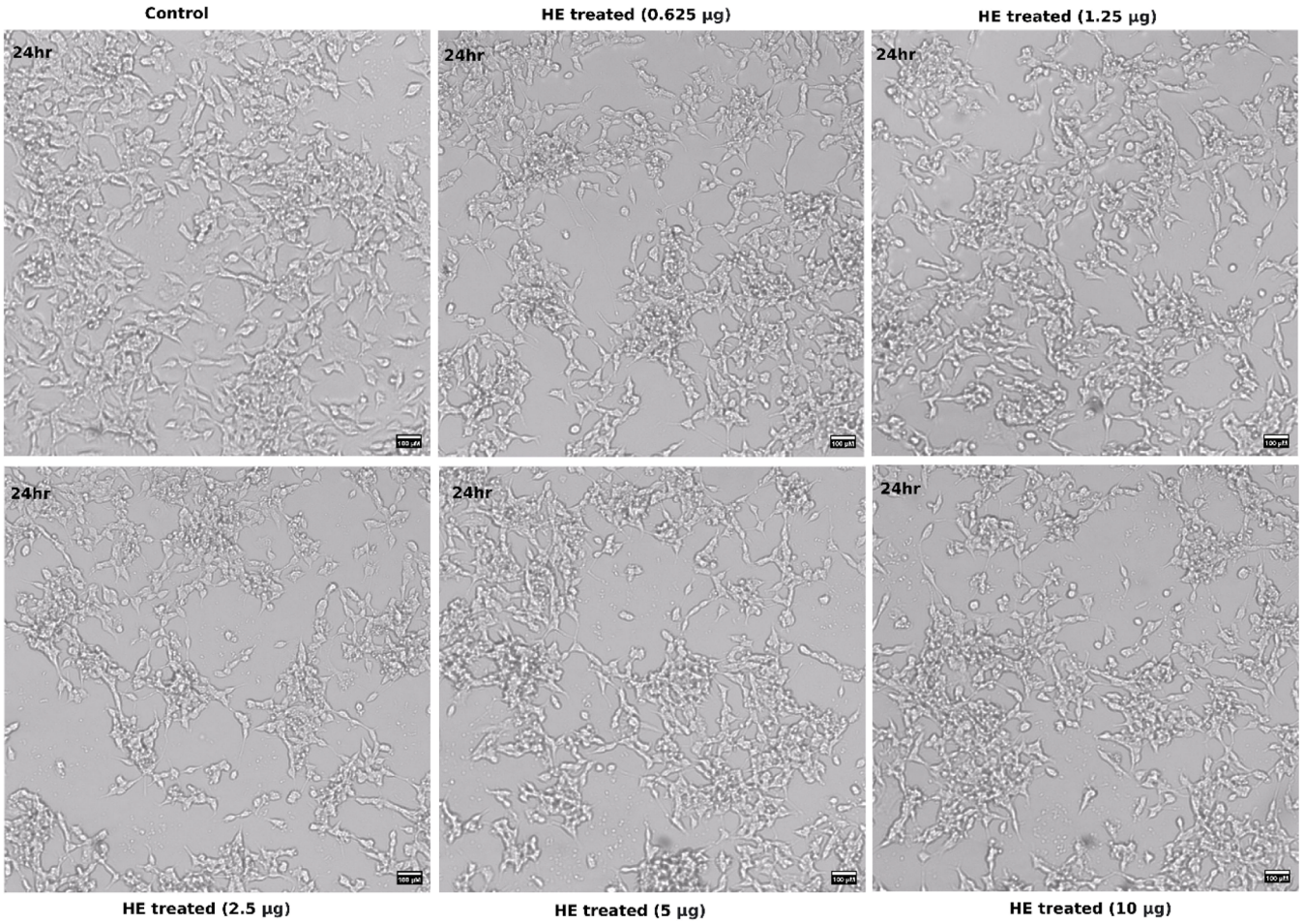

Figure 2. Morphological level examination of SH-SY5Y cells post-*Hericium erinaceus* treatment (0.625 to 10 μg/mL) revealing neuroprotective properties.

potential digestive and cardiovascular effects and several notable side effects like anxiety, sleep disturbances, depression, and even suicidal ideation. It often leads to recurrent symptoms upon cessation, contributing to poor patient adherence.[6] Therefore, there is an urgent need to explore potential drug targets specific to ADHD by harnessing the

https://doi.org/10.1021/acsomega.4c05522
ACS Omega 2025, 10, 4261−4275

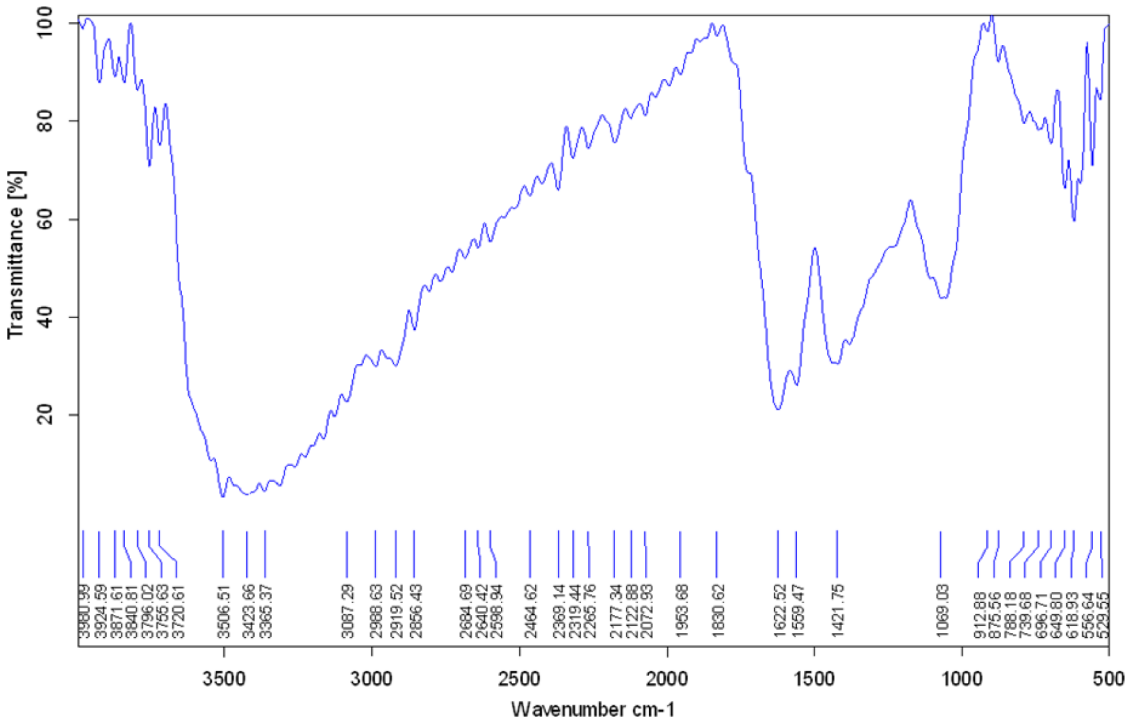

Figure 3. Fourier transform infrared spectrum of the aqueous extract of *Hericium erinaceus* in the presence of essential and diverse functional groups.

power of bioinformatics tools to comprehend molecular pathogenesis.[7] Concurrently, it remains crucial to design effective alternative medications for treating the disease.

Emerging evidence reports that herbal medicines derived from plant sources have been utilized for centuries, primarily to mitigate the side effects associated with synthetic drugs.[8] These compounds are recognized for their potential in various therapeutic areas, including antidiabetic, antioxidant, antimicrobial, antitumor, and anti-inflammatory effects.[9,10] Notably, mushrooms stand out as functional foods rich in nutrients and serve as reservoirs for novel therapeutic compounds.[11] Among the various culinary medicinal mushrooms, *Hericium erinaceus* or lion's mane has gained attention for its therapeutic potential in promoting brain and nerve health. It exhibits antihyperglycemic, antidiabetic, antioxidative, anti-inflammatory, anticancer, antimicrobial, and hypolipidemic effects.[12] For instance, Li et al. (2018) suggest that *H. erinaceus*-derived compounds can enhance the expression levels of neurotrophic factors.[13,14] Additionally, Chong et al. (2020) emphasize the therapeutic potential of *H. erinaceus* in treating several neurological conditions such as depressive disorder, cognitive impairment, and Alzheimer's and Parkinson's diseases.[12]

Herein, we aimed to assess the bioactive components of the *H. erinaceus* aqueous extract for their utility in the treatment of ADHD. The prepared aqueous extract of *H. erinaceus* exhibited noncytotoxic potential in human SH-SY5Y cell lines. Further, phytochemical screening, Fourier transform infrared spectroscopy (FTIR), and gas chromatography−mass spectrometry (GC−MS) analyses of the *H. erinaceus* extract confirmed the presence of the primary and secondary metabolites. Meanwhile, a series of computational methods were performed that identified established ADHD therapeutic targets. Further, GC−MS-identified *H. erinaceus* compounds were investigated against the therapeutic target through docking, molecular dynamics (MD), and quantum mechanics/molecular mechanics (QM/MM) studies.

2. RESULTS

2.1. Aqueous Extraction of *H. erinaceus* and Neuronal SH-SY5Y Cell Viability Post-treatment. Extracting *H. erinaceus* with an aqueous solvent via the Soxhlet method resulted in a yield of 21% dry extracted components. We investigated the cell viability effect of the *H. erinaceus* extract on SH-SY5Y cells. The cell viability assay relied on the reduction of MTT dye to formazan crystals by mitochondrial dehydrogenase. Results from the MTT assay indicate that the *H. erinaceus* extract at various concentrations (ranging from 0.625 to 10 μg/mL) exhibited minimal cytotoxicity on SH-SY5Y cells after a 24 h treatment period, demonstrating cell survival ability (Figure 1). Particularly, Figure 2 displays the post-treatment with the *H. erinaceus* extract at 0.625 to 10 μg/mL concentrations, and the SH-SY5Y cells exhibit no alterations in cell morphology or shrinkage through microscopic examination.

2.2. FTIR Spectrum Derived Functional Groups of the *H. erinaceus* Extract. The FTIR spectrum of the *H. erinaceus* aqueous extract (Figure 3) revealed major bands at 3720.61, 3506.51, 3423.66, 3365.37, 3087.29, 2684.69, 2598.94, 2265.76, 2122.88, 1953.68, 1830.62, 1622.52, 1559.47, 1069.03, 912.88, 875.56, 696.71, and 556.64 cm^{-1}. These band regions correspond to functional groups like alcohols/phenols, amines, aliphatic groups, aldehydes, carboxylic acids, nitriles, alkynes, allene, anhydrides, alkene, nitro compounds, mono/di/trisubstituted groups, and alkyl halides (Table 1).

2.3. Phytochemical Screening of the Extract. The preliminary phytochemical screening of the *H. erinaceus* extract showed the existence of carbohydrates, flavonoids, anthocyanins, tannins, alkaloids, steroids, and phenolic groups (Table 2). This diverse array of compounds suggests significant

https://doi.org/10.1021/acsomega.4c05522
ACS Omega 2025, 10, 4261−4275

Table 1. Functional Groups Identified with FT-IR Analysis in the Aqueous Extract of *Hericium erinaceus*

SI.No	Peak value	Band interaction	Functional group
1.	3720.61	O−H stretch	Alcohols, Phenols
2.	3506.51	N−H stretch	Amines
3.	3423.66	H-bonded	Phenols
4.	3365.37	O−H stretch	Alcohols
5.	3087.29	C−H stretch	Aliphatic groups
6.	2988.63	C−H stretch	Aliphatic groups
7.	2919.52	C−H stretch	Aliphatic groups
8.	2856.43	C−H stretch	Aliphatic groups
9.	2684.69	C−H stretch	Aldehydes
10.	2640.42	C−H stretch	Aldehydes
11.	2598.94	O−H stretch	Carboxylic acids
12.	2265.76	C≡N stretch	Nitriles
13.	2122.88	C≡C stretch	Alkynes
14.	1953.68	C═C═C stretch	Allene
15.	1830.62	C═O	Anhydrides
16.	1622.52	C═C	Alkene
17.	1559.47	NO_2 stretch	Nitro compounds
18.	1069.03	C−O stretch	Alcohols
19.	912.88	N−H wag	Primary and secondary amines
20.	875.56	C−H bend	Substituted groups
21.	788.18	C−H bend	Substituted groups
22.	696.71	−C≡C−H	Alkynes
23.	649.80	−C≡C−H	Alkynes
24.	618.93	−C≡C−H	Alkynes
25.	556.64	C−Br stretch	Alkyl halides
26.	529.55	C−Br stretch	Alkyl halides

Table 2. Qualitative Phytochemical Screening Results of *Hericium erinaceus*

SI.No	Phytochemicals	Aqueous extract
1	Carbohydrates	+
2	Flavanoids	+
3	Anthocyanins	+
4	Tannins	+
5	Alkaloids	+
6	Saponins	+
7	Steroids	+
8	Terpenoids	-
9	Triterpenoids	-
10	Diterpenes	-
11	Phenol	+
12	Proteins	-
13	Anthraquinone	-
14	Cholesterol	-
15	Phytosterol	-
16	Quinones	-
17	Coumarins	-
18	Emodin	-

medicinal potential, contributing to its extensive utilization in the drug and pharmaceutical industries. Conversely, terpenoids, triterpenoids, diterpenes, anthraquinones, cholesterol, phytosterols, quinones, coumarins, and emodins were notably absent from the extract.

2.4. *H. erinaceus* Metabolomics Profile. GC−MS analysis serves as a pivotal, sensitive, and precise method for metabolite profiling. Analysis of the *H. erinaceus* extract spectrum (Figure 4) revealed the presence of diverse compounds in the aqueous solvent fraction, with major phytochemical constituents identified as galactose methoxyamine (26.38%) with 17.6 retention time (RT). The other constituents obtained were glucose (18.76%), mannitol (11.41%), benzoic acid (6.42%), sucrose (6.41%), myo-inositol (5.47%), hexadecanoic acid (3.16%), glycerol (1.93%), butanedioic acid (0.75%), arabinose (0.68%), arabitol (0.64%), 1,3,5-tris(trimethylsiloxy)benzene (0.61%), threonic acid (0.33%), and benzene (0.23%) (Table 3).

2.5. Interaction Network for ADHD Drug Target Identification. Next, to explore the therapeutic utility of the *H. erinaceus* compounds in ADHD conditions, we identified the genes that are functionally expressed and highly reported in ADHD by a comprehensive exploration from the GeneCards and DisGeNet databases. After applying the threshold criteria, we retrieved a compiled list of 7895 unique genes by integrating 7053 ADHD-specific genes from GeneCards and 842 genes from DisGeNet. After data curation, a final data set of 7234 unique genes that were associated with ADHD conditions was compiled to generate a protein interaction network using Cytoscape 3.9.1. The resulting network displayed 5811 nodes and 225672 edges, which offers insight into the functional relationships between the ADHD-associated genes encoding proteins in disease conditions. From the network, the highly interconnected clusters were extracted utilizing the MCODE algorithm. Among them, the top-ranked ten clusters (Table S1) exhibiting dense connectivity were selected (Figure 5A−J). The ontological assessment confirmed that these selected ten clusters participate profoundly in the regulation of the MAPK pathway, Ras signaling, TNF signaling, stress response, response to stimuli, neurodegenerative disease pathways, neuroactive ligand−receptor interaction, glutamatergic synapse, dopaminergic synapse, synaptic signaling, serotonergic synapse, chemical synaptic transmission, and GABAergic synapse (Table S1).

2.6. Mapping Well-Known ADHD Therapeutic Protein Targets from Significant Clusters. Following an extensive search through the TTD, ChEMBL, and DrugBank databases, a comprehensive list comprising over 147 established ADHD protein targets was compiled. Subsequently, these well-known targets were mapped within the selected top ten clusters, revealing nine clusters with the presence of ADHD protein targets. Notably, 44 established ADHD protein targets were distributed among the ten clusters (Table 4). Using the ten selected clusters, the subnetwork (Figure 6A) was constructed via the STRING database. Further, the CytoHubba plug-in was used that pinpointed SLC6A4 as a candidate therapeutic target displaying a high degree of connectivity (n = 9) among the subnetwork (Figure 6B).

2.7. Molecular Docking of GC−MS Derived Compounds Against SLC6A4 Target. The molecular docking was performed using the GC−MS-derived compounds from the *H. erinaceus* aqueous extract against the SLC6A4 target. The three-dimensional structure of SLC6A4 was obtained through the accession ID: 5I6X, which comprised the human serotonin transporter in complex with paroxetine, a serotonin reuptake inhibitor. The active pocket residues were set at TYR95, ALA96, ASP98, ALA169, ILE172, ALA173, TYR176, PHE335, SER336, GLY338, PHE341, SER438, SER439, GLY442, and VAL501, ligand (paroxetine) binding sites in order to block the activity of SLC6A4. The molecular docking calculations were performed in extra precision mode using

https://doi.org/10.1021/acsomega.4c05522
ACS Omega 2025, 10, 4261−4275

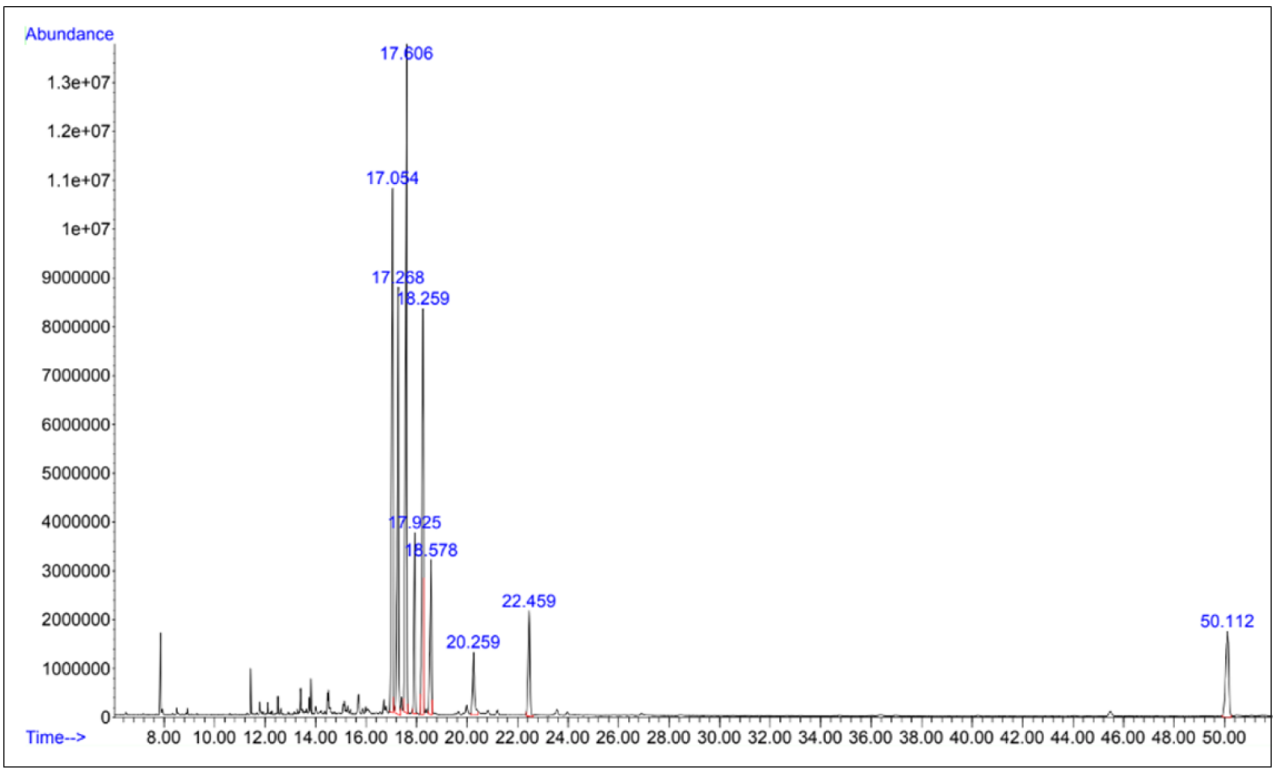

Figure 4. GC−MS Chromatogram of the aqueous extract of *Hericium erinaceus* displaying 17 bioactive components.

Table 3. GC−MS Analysis of the *Hericium erinaceus* Extract

SI. No	Retention time (min)	Phytocompounds	Molecular formula	Area (%)
1	7.858	Glycerol, tris-TMS ether	$C_{12}H_{32}O_3Si_3$	1.938
2	11.430	Bis(trimethylsilyl) 2-[(trimethylsilyl)oxy]succinate	$C_{13}H_{30}O_5Si_3$	0.759
3	11.787	Threitol	$C_{16}H_{42}O_4Si_4$	0.332
4	12.111	1,2,3-Tris(trimethylsiloxy)benzene	$C_{15}H_{30}O_3Si_3$	0.235
5	12.506	Threonic acid	$C_{16}H_{40}O_5Si_4$	0.337
6	13.406	1,3,5-Tris(trimethylsiloxy)benzene	$C_{15}H_{30}O_3Si_3$	0.619
7	13.820	Arabinose	$C_{18}H_{45}NO_5Si_4$	0.684
8	14.511	Arabitol	$C_{20}H_{52}O_5Si_5$	0.643
9	15.697	Trimethylsilyl 3,4-bis(trimethylsilyloxy)benzoate	$C_{16}H_{30}O_4Si_3$	0.756
10	17.054	Fructose	$C_{22}H_{55}NO_6Si_5$	18.760
11	17.268	Fructose	$C_{22}H_{55}NO_6Si_5$	15.657
12	17.606	Galactose methoxyamine	$C_{22}H_{55}NO_6Si_5$	26.389
13	18.235	Mannitol	$C_{24}H_{62}O_6Si_6$	11.410
14	18.578	Trimethylsilyl 3,4,5-tris[(trimethylsilyl)oxy]benzoate	$C_{19}H_{38}O_5Si_4$	6.429
15	20.259	Hexadecanoic acid	$C_{19}H_{40}O_2Si$	3.167
16	22.459	Myo-inositol TMS	$C_{24}H_{60}O_6Si_6$	5.474
17	50.112	Sucrose	$C_{36}H_{86}O_{11}Si_8$	6.412

these GC−MS-derived compounds (n = 17) against SLC6A4. Our analysis identified myo-inositol with the highest binding affinity against SLC6A4, with an energy value based on the glide score of −6.53 kcal/mol (Table 5), while other compounds were found to exhibit binding affinities between the ranges of −5.93 to −4.20 kcal/mol (Table 5). The myo-inositol formed two hydrogen bonds at ASP98 and a single hydrogen bond at TYR95 and PHE335 active pocket residues, as depicted in Figure 7.

2.8. Interactive Stability of Complex in the Dynamic Environment throughout 100 ns. Molecular dynamics simulation was executed to assess the conformational stability of the myo-inositol with SLC6A4 over 100 ns. The RMSD plot depicted minimal fluctuation initially and then attained a stable equilibrium, indicating the sustained binding of myo-inositol with SLC6A4 protein throughout the simulation period. The average root-mean-square deviations (RMSD) of the complex were notably low (2.33 Å), ensuring stable interaction (Figure 8A). Likewise, the root-mean-square fluctuations (RMSF) plot offers valuable information about the flexibility of individual amino acids throughout the simulation period of 100 ns. The RMSF analysis was conducted for both undocked SLC6A4 and myo-inositol-docked SLC6A4 complex. Upon binding with myo-inositol, the RMSF profile of SLC6A4 showed reduced fluctuations, especially in the regions surrounding the binding sites like ASP98, TYR95, and PHE335, ranging narrowly

https://doi.org/10.1021/acsomega.4c05522
ACS Omega 2025, 10, 4261−4275

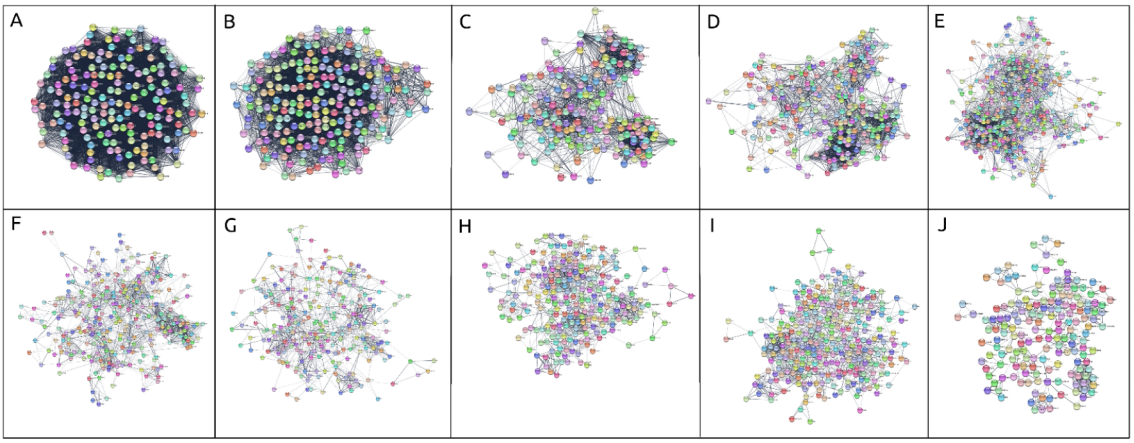

Figure 5. Top ten (A–J) densely interconnected significant subnetworks obtained from MCODE, Cytoscape.

between 0.52 and 0.62 Å (Figure 8B). Furthermore, protein–ligand interaction plots illustrated the highest occurrence of hydrogen bonds and water bridge interactions originating from the binding pocket residues such as ASP98, TYR95, and PHE335 (Figure 8C). These factors ensure the stable binding of myo-inositol with the SLC6A4 target.

2.9. Quantum-Based Frontier Molecular Orbitals Iso-surface and MESP Contour Map of Myo-Inositol into the Active Pockets of SLC6A4. In QM/MM calculations, we optimized the myo-inositol-SLC6A4 complex using the B3LYP/6-31*G basic set. The frontier molecular orbitals, including HOMO and LUMO, provide insight into electron-donating/accepting potential and highlight key reactive regions within the protein–ligand complex.[15] The blue region denotes an electrostatically positive region, while the red color represents a negative electrostatic potential region.[16] Figure 9A,B illustrates the HOMO and LUMO iso-surfaces, which reveal the electrophilic and nucleophilic regions of myo-inositol interacting with ASP98, TYR95, and PHE335 active residues of SLC6A4. Furthermore, the MESP (Figure 9C) surface represents both electropositive and electronegative regions of myo-inositol for stable binding with the active pocket of the target protein. Overall, the QM/MM results affirm a stable interaction between myo-inositol and SLC6A4.

3. DISCUSSION

ADHD is primarily seen as a childhood behavioral condition that has significant social and economic consequences.[4] It is influenced by a complicated interaction of genetic, neurological, and environmental variables.[17] Increasing data has indicated that over 50% of individuals with ADHD experience symptoms persisting into adulthood and perhaps for the duration of their entire lives.[18] The intricate complex origin and development of the disease have made it difficult to identify crucial treatment strategies.[19] Among the variety of established ADHD treatments, methylphenidate and amphetamines are commonly used, yet these medications pose significant adverse and lethal effects.[20] Mushrooms, including *H. erinaceus*, have emerged as highly promising prospects for medication development in the field of alternative medicine.[21] According to Brandalise et al. (2023), bioactive compounds derived from *H. erinaceus* have been found to be effective in treating several neuropsychiatric disorders such as depression, Alzheimer's disease, Parkinson's disease, and spinal cord injury.[22] Similarly, Szućko-Kociuba et al. (2023) have highlighted that neuroprotective effects of *H. erinaceus* have the ability to stimulate the growth of neuronal cells, prevent neuronal cell death, and facilitate the regeneration of neurons.[23] Thus, our study sought to isolate and characterize putative bioactive chemicals from *H. erinaceus* through a series of experimental investigations along with a rigorous computational investigation to discover promising drug candidates and therapeutic targets in ADHD treatment. Following the Soxhlet-mediated extraction of *H. erinaceus* in an aqueous fraction, the dried extract was subjected to a cytotoxicity assay in cultivated SH-SY5Y cells. Using the *H. erinaceus* extract at concentrations of 0.625, 1.25, 2.5, 5, and 10 μg/mL for a duration of 24 h did not show any harmful effects on cells (Figure 1). This was confirmed by observing that there were no changes in cell morphology under a microscope (Figure 2). Further, FTIR spectroscopy (Figure 3) was utilized to determine the functional groups of the active components by examining the IR bands. The FTIR spectra confirmed the presence of several functional groups, including alcohols/phenols, amines, aliphatic groups, aldehydes, carboxylic acids, nitriles, alkynes, allene, anhydrides, alkene, nitro compounds, mono/di/trisubstituted groups, and alkyl halides (Table 1). Subsequently, the phytochemical screening analysis revealed the presence of carbohydrates, flavonoids, anthocyanins, tannins, alkaloids, saponins, steroids, and phenolic groups (Table 2) that align with the results of the FTIR functional group assignment of the extract. According to Baishya et al. (2024), the presence of these phytochemicals in *H. erinaceus* confers antimicrobial, antioxidant, antifungal, anti-inflammatory, anti-allergenic, antiviral, hepatoprotective, anti-inflammatory, anti-carcinogenic, antithrombic, and analgesic effects.[24] Further, the metabolite profiling through GC–MS analysis of the *H. erinaceus* extract spectrum identified the existence of 17 chemicals in the aqueous fraction. The confirmation of chemical constituent identification was based on the analysis of the molecular weight, retention time, and molecular formula. The examination of *H. erinaceus* using GC–MS chromatography (Figure 4) revealed the presence of active chemicals, which are reported in Table 3. The primary phytochemical ingredients found include galactose methoxyamine, glucose, mannitol, benzoic acid, sucrose, myo-inositol, hexadecanoic acid, glycerol, butanedioic acid, arabinose, arabitol, 1,3,5-tris(trimethylsiloxy)benzene, threonic acid, and benzene.

https://doi.org/10.1021/acsomega.4c05522
ACS Omega 2025, 10, 4261–4275

Table 4. List of Mapped ADHD Protein Targets Distributed among Significant Nine Clusters of the Network

	Drug Targets	
SI. No	Gene symbol	Protein Name
1	ESR1	Estrogen Receptor 1 (Alpha)
2	ESR2	Estrogen Receptor 2
3	NTRK1	Neurotrophic Receptor Tyrosine Kinase 1
4	MAD2L2	Mitotic Arrest Deficient 2 Like 2
5	FGFR1	Fibroblast Growth Factor Receptor 1,
6	ABCB1	ATP Binding Cassette Subfamily B Member 1
7	FGFR2	Fibroblast Growth Factor Receptor 2
8	AIM2	Absent In Melanoma 2
9	FGFR4	Fibroblast Growth Factor Receptor 4
10	PTGDR2	Prostaglandin D2 Receptor 2
11	FGFR3	Fibroblast Growth Factor Receptor 3
12	C5AR1	Complement C5a Receptor 1
13	KCNA1	Potassium Voltage-Gated Channel Subfamily A Member 1
14	KCND2	Potassium Voltage-Gated Channel Subfamily D Member 2
15	KCND3	Voltage-Gated Potassium Ion Channel Subfamily D Member 3
16	KCNQ2	Potassium Voltage-Gated Channel Subfamily Q Member 2
17	KCNQ3	Potassium Voltage-Gated Channel Subfamily Q Member 3
18	NTRK2	Neurotrophic Receptor Tyrosine Kinase 2
19	CTSK	Cathepsin K
20	ADRB2	Adrenoceptor Beta 2
21	CHRM2	Cholinergic Receptor Muscarinic 2
22	OPRD1	Opioid Receptor Delta 1
23	ABCB11	ATP Binding Cassette Subfamily B Member 11
24	CTSL	Cathepsin L
25	CYP2D6	Cytochrome P450 Family 2 Subfamily D Member 6
26	DRD1	Dopamine Receptor D1
27	KCNH2	Potassium Voltage-Gated Channel Subfamily H Member 2
28	OPRM1	Opioid Receptor Mu 1
29	F10	Coagulation Factor X
30	CYSLTR1	Cysteinyl Leukotriene Receptor 1
31	CARTPT	Cocaine And Amphetamine-Regulated Transcript Prepropeptide
32	HTR3A	5-Hydroxytryptamine Receptor 3a
33	MAOA	Monoamine Oxidase A
34	MAOB	Monoamine Oxidase B
35	SLC6A3	Solute Carrier Family 6 Member 3
36	ASH1L	Ash1 Like Histone Lysine Methyltransferase
37	ADRA2B	Adrenoceptor Alpha 2B
38	ADRA2C	Adrenoceptor Alpha 2C
39	GRIN1	Glutamate Ionotropic Receptor NMDA Type Subunit 1
40	KCNJ3	Potassium Inwardly Rectifying Channel Subfamily J Member 3
41	TBXA2R	Thromboxane A2 Receptor
42	ADRA1A	Adrenoceptor Alpha 1A
43	ADRA1D	Adrenoceptor Alpha 1d
44	SLC6A4	Solute Carrier Family 6 Member 4

Subsequently, the identified GC−MS compounds of the *H. erinaceus* aqueous extract were utilized to determine their therapeutic potential against potential targets expressed in ADHD conditions. In accordance with Chen et al. (2023), we have employed comprehensive multiomics and computational workflows to discover specific ADHD targets.[25] Using computational methods, we compiled 7,234 genes associated with ADHD from multiple databases. Next, we examined their protein connectivity to better understand the functional interactions that underlie ADHD and determine the potential therapeutic targets. Our constructed protein network consists of 5,811 nodes and 225,672 edges. Subsequently, we analyzed the ADHD network and dissected it into several clusters, each reflecting essential functional components with densely connected proteins. Top ten clusters (Figure 5A−J) were selected based on their high connectivity and then mapped with previously established ADHD therapeutic protein targets (n = 147). The analysis showed that 44 known protein targets were distributed among all ten clusters, as shown in Table 4. Further, the ontological examination showed a significant role of these ten clusters in biological processes as well as molecular pathways (Table S1). As a result, cluster 1 significantly participated in response to stimuli, stress response, response to chemical stimuli, apoptosis, response to cytokine, JAK-STAT signaling, cytokine-cytokine receptor interactions, and TNF signaling. While clusters 2−4 were enriched in functions like response to stimuli, stress response, response to chemical stimuli, response to organic substances, MAPK signaling, cytokine-cytokine receptor interactions, JAK-STAT signaling, chemokine signaling, T-cell receptor signaling, and RAS signaling. Clusters 5−9 were found to be prominently involved in neurodegenerative disease pathways, Huntington's disease, Alzheimer's disease, amyotrophic lateral sclerosis, endocytosis, neuroactive ligand−receptor interaction, glutamatergic synapse, MAPK signaling, dopaminergic synapse, adrenergic signaling, GABAergic synapse, cell−cell signaling, synaptic signaling, and chemical synaptic transmission. The cluster 10 proteins cooperatively function in MTOR signaling, oxytocin signaling, synaptic vesicle cycle, cardiomyopathy, and metabolic pathways. All these pathways and molecular processes have been previously identified as dysregulated in ADHD. For instance, Bollmann et al. (2015) correlate the increased levels of gamma-aminobutyric acid in ADHD conditions, while Schnorr et al. (2024) clearly present increased TNF signaling and inflammatory markers in ADHD.[26,27] Recently, Becker et al. (2021) provide the neurodegeneration risk susceptibility in ADHD individuals.[28] Furthermore, Bauer et al. (2018) and Zhong et al. (2023) have emphasized the risk of ADHD genes causing the impaired glutamatergic and dopaminergic synapse in ADHD disease progression.[29,30] Hence, identifying the therapeutic target within clusters regulating these functional mechanisms will be promising for enhancing ADHD treatment strategies.

Further, using the 44 established targets observed among the ten clusters, a subnetwork was generated that ultimately depicts the ADHD therapeutic target proteins (Figure 6A). By using Cytohubba on the subnetwork, the SLC6A4 protein is found to be a potential target that connects multiple established ADHD protein targets such as ESR1, CYP2D6, KCNH2, SLC6A3, OPRM1, MAOA, NTRK2, DRD1, and ADRB2 (Figure 6B). Pinsonneault et al. (2017) suggested that ESR1 plays a role in behavioral disorders.[31] Dean (2020) established a correlation between the CYP2D6 target and the ADHD medicine atomoxetine.[32] Henningsson et al. (2015) emphasized the significance of KCNH2 in the formation and retention of social memory.[33] Reith et al. (2022) presented evidence supporting the role of SLC6A3 as a promising target for pharmacological treatment in ADHD.[34] Carpentier et al. (2013) highlighted the significance of OPRM1 in ADHD.[35]

https://doi.org/10.1021/acsomega.4c05522
ACS Omega 2025, 10, 4261−4275

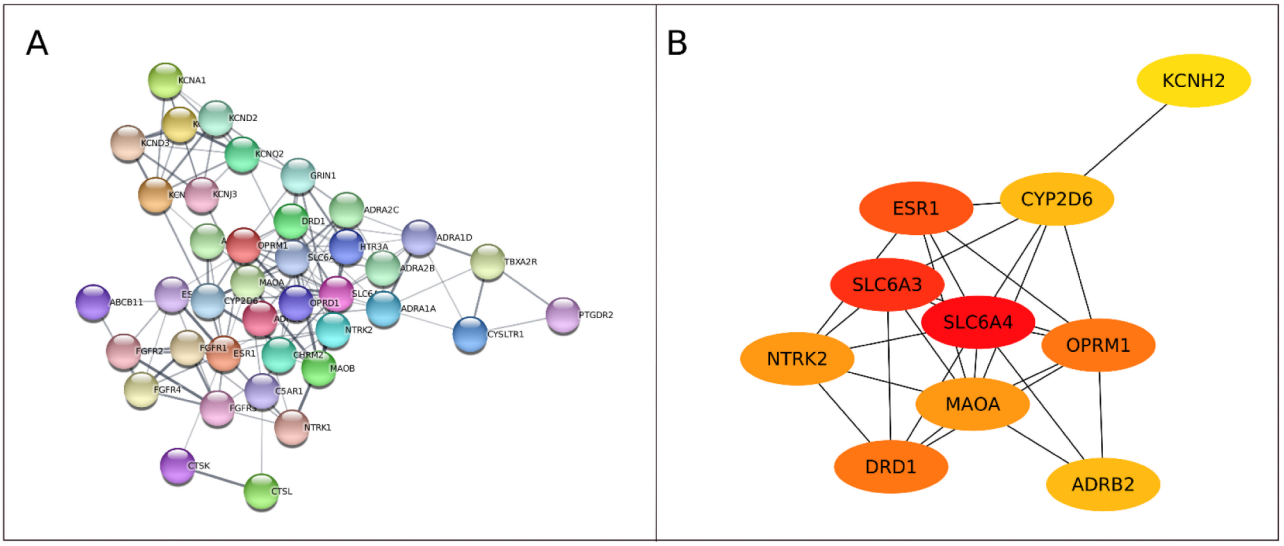

Figure 6. (A) ADHD drug targets subnetwork employing ten clusters; (B) SLC6A4 as the central component exhibiting high nodal connectivity among other ADHD drug targets.

Table 5. Binding Energy of Top Five Compounds Derived from the HE Extract against SLC6A4

Sl.NO	HE extract compounds	PubChem ID	Glide score (kcal/mol)
1	Myo-inositol TMS	520232	−6.53
2	Hexadecanoic acid, trimethylsilyl ester	521638	−5.93
3	1,3,5-Tris(trimethylsiloxy)benzene	517874	−4.52
4	Trimethylsilyl 3,4-bis(trimethylsilyloxy)benzoate	520055	−4.41
5	Trimethylsilyl ether of glycerol	522285	−4.20

Kwon et al. (2014) found a correlation between variations in the MAOA gene and ADHD.[36] Ribasés et al. (2008), Mariggiò et al. (2021), and Glessner et al. (2023) have presented evidence supporting the importance of NTRK2, DRD1, and ADRB2, respectively, in the context of ADHD.[37−39]

Then, the compounds determined through GC−MS analysis were used to evaluate their suitability as drugs for ADHD by targeting the discovered SLC6A4. Out of the 17 compounds, myo-inositol displayed the most binding affinity toward SLC6A4 by forming two hydrogen bonds at ASP98 and one hydrogen bond at TYR95 and PHE335 active pocket residues (Figure 7), resulting in an energy value of −6.53 kcal/mol (Table 5). This strong binding indicates that myo-inositol holds potential inhibitory ability against the SERT (Serotonin transporter) (encoded by SLC6A4) to inhibit its function and ultimately increase serotonin levels in the brain for ADHD treatment. Myo-inositol is an isomer of inositol, which is a naturally occurring molecule that resembles simple sugar. Increasing evidence like Mancini et al. (2016) revealed the efficacy of myo-inositol in ameliorating insulin resistance in obese youngsters.[40] In addition, Kalra et al. (2016) suggest the use of inositol for the treatment of polycystic ovarian syndrome.[41] López-Gambero et al. (2020) suggested that myo-inositol demonstrates effectiveness in treating depression, anxiety, and obsessive behaviors.[42] Subsequently, the MD simulation experiment conducted over a duration of 100 ns demonstrated that the target protein exhibited a consistent RMSD and maintained equilibrium throughout 100 ns. While, the RMSF plot of SLC6A4 in complex with myo-inositol revealed reduced residual fluctuations at the active pocket residues ASP98, TYR95, and PHE335 when compared to the undocked SLC6A4, as illustrated in Figure 8A,B. The interaction plots demonstrate the involvement of hydrogen bonds and water bridge interactions by the ASP98, TYR95, and PHE335 residues in enhancing the binding affinity of myo-inositol (Figure 8C). Therefore, our research demonstrates that the ASP98, TYR95, and PHE335 residues play a critical role in the inhibition of SLC6A4 by myo-inositol. Furthermore, electron transfer abilities denoted by electropositive and electronegative regions were observed in the HOMO, LUMO, and MESP contour maps, indicating the formation of stable hydrogen bonds with the target ASP98, TYR95, and PHE335 residues of SLC6A4 (Figure 9A−C). As a result, our docking, dynamic simulation, and QM/MM findings are in correlation with each other. Our study demonstrates that myo-inositol, extracted from the aqueous solution of *H. erinaceus*, exhibits an inhibitory effect on the SLC6A4. This interaction suggests a promising capability to regulate the imbalanced synaptic transmission that is often linked to ADHD. Overall, our comprehensive computational and experimental research highlights and indicates the effectiveness of myo-inositol as a possible medication targeting SLC6A4 in individuals with ADHD.

4. MATERIALS AND METHODS

4.1. Chemicals, Reagents, and Instrumentation. All chemicals utilized in this study, including glacial acetic acid, ammonia, hydrochloric acid, sulfuric acid, acetone, Benedict's reagent, Molisch reagent, sodium hydroxide, ferric chloride, iodine, potassium iodide, ninhydrin, copper acetate, and potassium bromide, were procured from HIMEDIA (Bangalore, India). Dimethyl sulfoxide (DMSO), *N*-methyl-*N*-(trimethylsilyl)trifluoroacetamide (MSTFA), methoxyamine hydrochloride, penicillin/streptomycin, and 2,2-diphenyl-1-picrylhydrazyl (DPPH) were obtained from Sigma-Aldrich, St. Louis, USA. All chemicals and reagents were of analytical grade. Cell culture grade, Ham's F12, Dulbecco's Modified Eagle Medium (DMEM), 3-(4,5-dimethylthiazol-2-yl)-2,5-diphenyltetrazolium bromide (MTT), Fetal Bovine Serum (FBS), and Dulbecco's Phosphate-Buffered Saline (D-PBS)

https://doi.org/10.1021/acsomega.4c05522
ACS Omega 2025, 10, 4261−4275

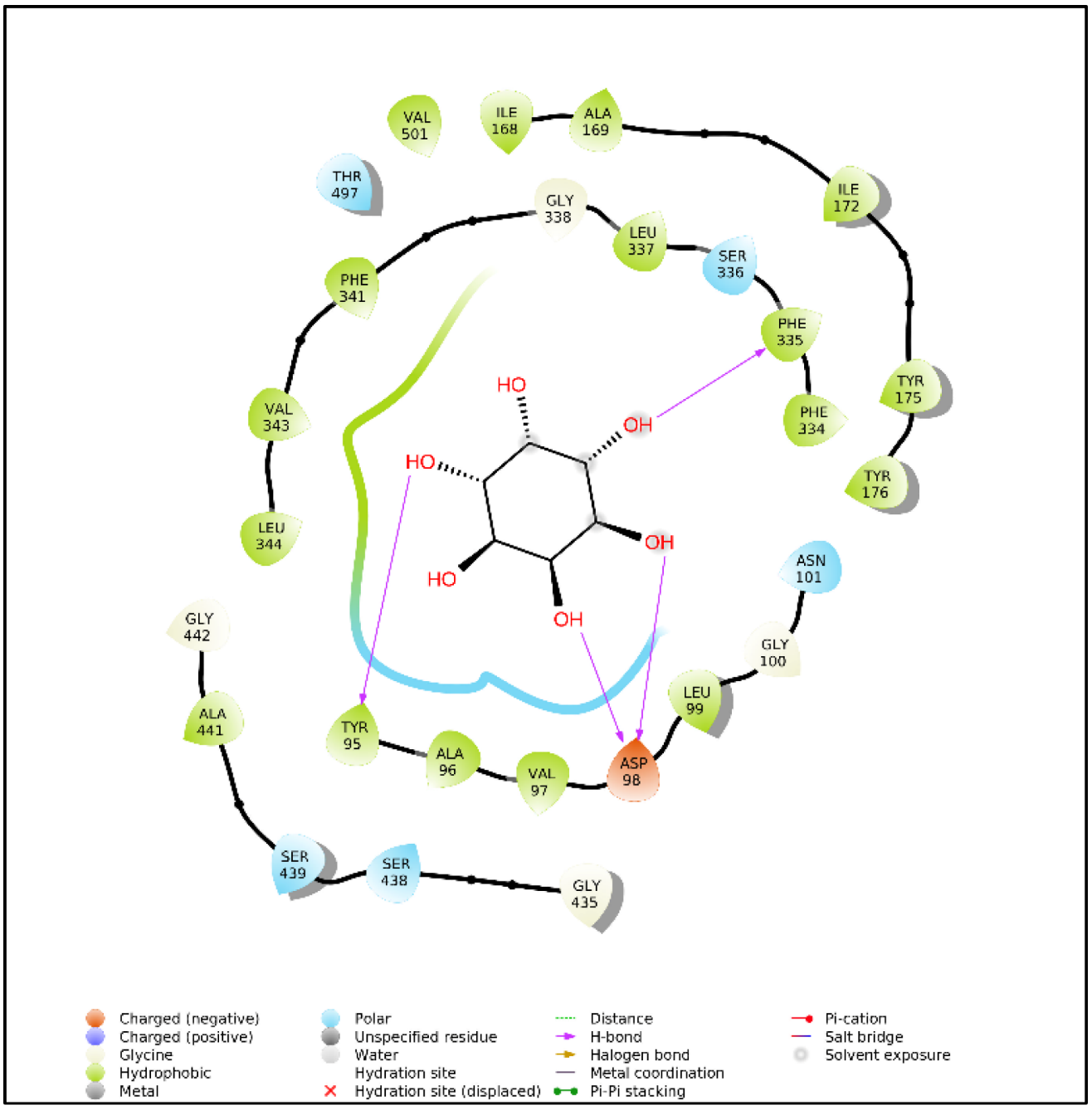

Figure 7. Hydrogen bonds formed at TYR95, ASP98, and PHE335 residues of SLC6A4 post-molecular docking with myo-inositol.

were acquired from HIMEDIA (Bangalore, India). The instruments employed for determining neuroprotective effects and functional groups in the *H. erinaceus* extract include UV−visible spectrophotometry (Shimadzu UV 1800), Whatman filter paper (No. 1), centrifuge (Remi: R-8C), inverted binocular biological microscope (Olympus, USA), biosafety hood (Precision Scientific, Chennai), 37 °C incubator with a humidified atmosphere of 5% CO2 (ThermoFisher, USA), 96-well plate reader (EPOCH2, BioTek, CA, USA), Bruker Alpha FTIR spectrometer (Bruker Optics GmbH, Ettlingen, Germany), and gas chromatography−mass spectrometry (GC−MS, Shimadzu GCMS-QP2010, Kyoto, Japan).

4.2. *H. erinaceus* Collection and Aqueous Extraction. The use of *H. erinaceus* in our study complied with the institutional guidelines. The farm-fresh mushroom *H. erinaceus* (commonly known as LION'S Mane) was purchased from Green Apron India. The *H. erinaceus* fruiting body was carefully rinsed with distilled water to eliminate debris and dust particles, air-dried thoroughly, and then ground to a fine powder. Fifty grams of air-dried fruiting body powder was mixed in 500 mL of hot distilled water and subjected to extraction using the Soxhlet extraction method for 18 h. The resulting extracts were filtered, and the solvent was concentrated using fractional distillation at 45 °C until complete dryness. We then stored the dried plant extracts at 4 °C for subsequent analysis.

4.3. Culturing SH-SY5Y Neuroblastoma Cell Lines. The human SH-SY5Y neuroblastoma cells were acquired from the National Centre for Cell Sciences (NCCS) in Pune, India. These cells were cultured in DMEM/F-12 in a 1:1 ratio. The

https://doi.org/10.1021/acsomega.4c05522
ACS Omega 2025, 10, 4261−4275

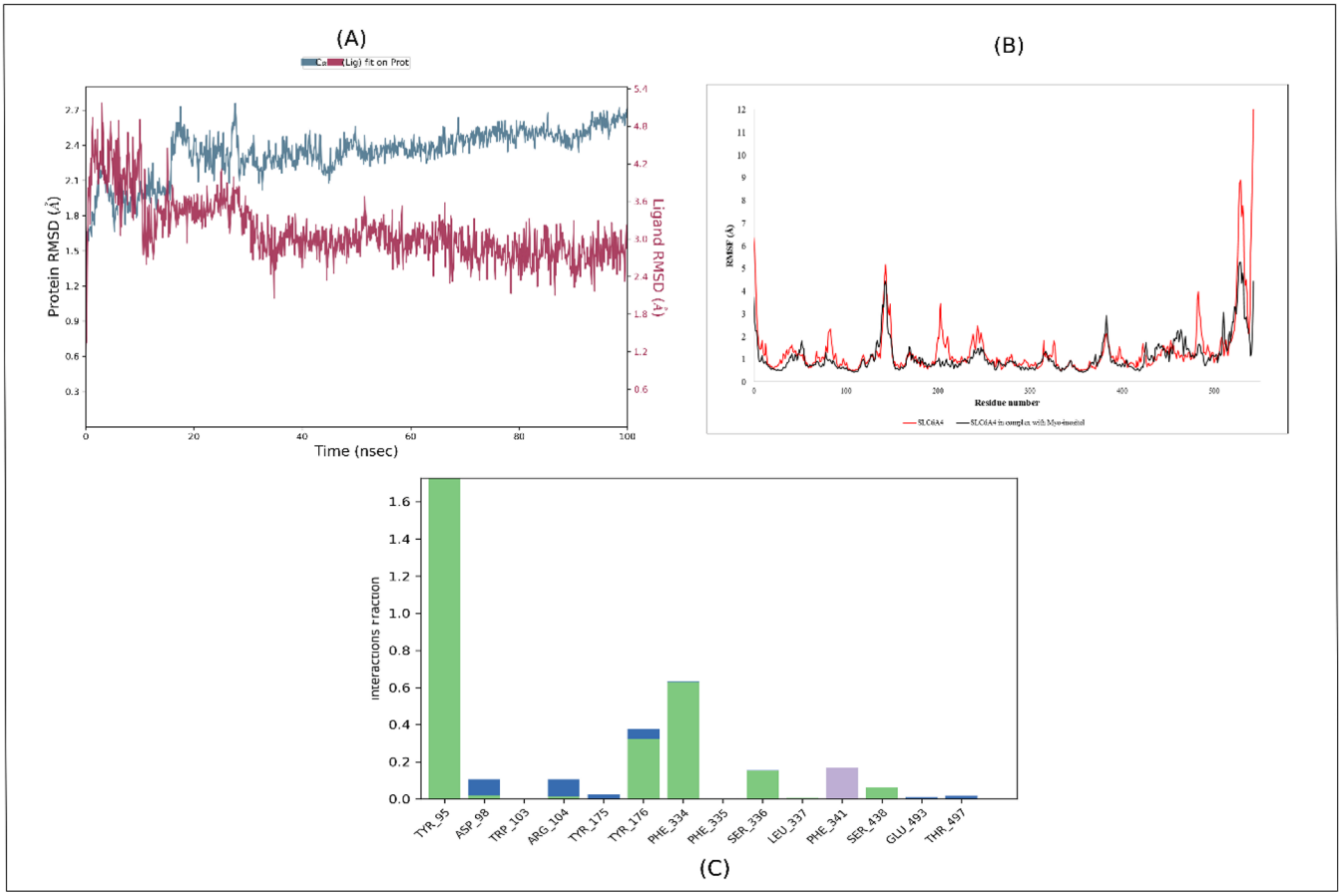

Figure 8. (A) RMSD analysis of free SLC6A4 (blue) and post binding with myo-inositol (red) throughout 100 ns; (B) target SLC6A4 RMSF analysis pre- and post-myo-inositol binding for 100 ns; (C) hydrogen (green), hydrophobic (purple), and water bridge (blue) interactions formed between myo-inositol and SLC6A4.

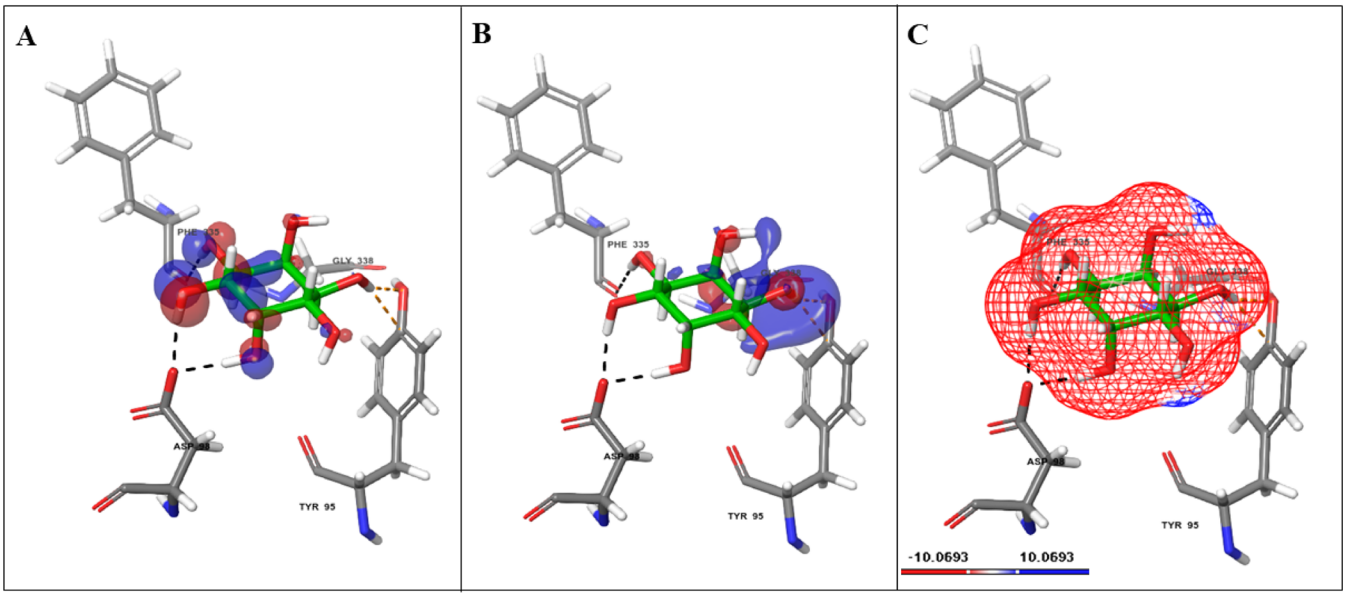

Figure 9. (A) Electron donating region of myo-inositol at TYR95, ASP98, and PHE335 residues of SLC6A4; (B) electron accepting region of myo-inositol at TYR95, ASP98, and PHE335 residues of SLC6A4; (C) Poisson−Boltzmann electropositive and electronegative regions of myo-inositol binding at TYR95, ASP98, and PHE335 residues of SLC6A4.

culture medium was supplemented with 0.1 mM nonessential amino acids, 1.5 g/L sodium bicarbonate, 1 mM sodium pyruvate, 10% FBS, and a 1% antibiotic-antimycotic solution. The cells were preserved in a controlled CO_2 incubator with 5% CO_2, and 18−20% O_2, at 37 °C. Subculturing of cells was accomplished every 2 days to ensure their healthy growth and

https://doi.org/10.1021/acsomega.4c05522
ACS Omega 2025, 10, 4261−4275

maintenance. Then, SH-SY5Y cells were trypsinized and resuspended in a medium before plating at a density of 20,000 cells/well in a 96-well plate. Following a 24 h incubation period, the cells were utilized for subsequent investigations.

4.4. Effect of the *H. erinaceus* Aqueous Extract on SH-SY5Y Cells. The SH-SY5Y cell lines were subjected to a cellular viability assay to assess cytotoxicity effects of *H. erinaceus* as described by Lazarova et al. (2024).[43] Following a 24 h incubation period with 5% CO_2 and 37 °C, the cell lines were exposed to various concentrations (0.625, 1.25, 2.50, 5.00, and 10.00 μg/mL) of the *H. erinaceus* aqueous extracts. The negative control consisted of cells that were not exposed to any extract. Subsequently, the culture medium was aspirated, and 0.5 mg/mL MTT solution was added, followed by an additional 3 h incubation. Then, the MTT solution was carefully discarded, and 100 μL of DMSO was added to dissolve the formed crystals. After agitating the plate for 1 min, we measured the formazan absorbance in each well at 570 nm using a microplate reader. The percentage of cell viability was calculated utilizing the following equation:

$$\%\ \text{Cell Viability} = \frac{\text{O. D}_{\text{treatment}}}{\text{O. D}_{\text{control}}} \times 100$$

4.5. Fourier Transform Infrared Spectroscopic Analysis of Extract. FTIR analysis was employed to identify the functional groups within the *H. erinaceus* extract, which offers a powerful method for identifying chemical components by analyzing the absorption bands of different molecular groups. The wavelength and intensity of these bands provide valuable insights into the sample composition. Initially, 10 mg of extract was encapsulated uniformly in a 100 mg KBr pellet to create translucent discs. These discs were then subjected to FTIR spectroscopy, and the spectra were recorded within the absorption range of 4000 to 500 cm^{-1}.

4.6. Preliminary Qualitative Screening of Phytochemicals. *H. erinaceus* plant extract was subjected to phytochemical screening by various phytochemical tests such as carbohydrates, flavonoids, alkaloids, anthocyanins, tannins, saponins, terpenoids, steroids, triterpenoids, phenols, diterpenes, anthraquinones, cholesterol, phytosterols, quinones, coumarins, and emodins, as described by Shaikh et al. (2020).[44] The presence of phytochemicals was determined by visually examining the color or frothing.

4.7. Preparation and Derivatization of Samples for GC−MS Analysis. A two-step derivatization procedure was applied to the *H. erinaceus* extract prior to GC−MS analysis.[45] Briefly, 50 μL of pyridine was mixed with 10 mg of extract and sonicated for 5 min. Subsequently, 100 μL of methoxyamine hydrochloride (20 mg/mL) in pyridine was added to the extract solution, which was then incubated in a shaker at 100 rpm, 60 °C for 2 h. Following this, 300 μL of MSTFA was added to the mixture and incubated for 30 min under the same conditions. Then, the derivatized sample was filtered using a syringe filter of 0.45 μm, sealed with aluminum foil, and allowed to stand at 37 °C overnight.

4.8. Gas Chromatography−Mass Spectrometry (GC−MS) Analysis. After derivatization, one microliter of the derivatized samples underwent injection in the splitless mode into a GC−MS system (Shimadzu GCMS-QP2010, Kyoto, Japan). The *H. erinaceus* aqueous extract underwent separation on a DB-5MS 5% phenyl methyl siloxane column with an inner diameter of 250 μm and a film thickness of 0.25 μm (Agilent Technologies, Santa Clara, CA, USA), utilizing helium as the carrier gas at a flow rate of 1 mL/min. The initial oven temperature was established at 100 °C for 5 min, followed by sequential increments to a target temperature of 190 °C at 10 °C/min, then to 204 °C at 1 °C/min, and ultimately to 325 °C at 2 °C/min with a total run time of 88.5 min. The injector and ion source temperatures were maintained at 250 and 230 °C, respectively. The relative percentage of each compound was determined by normalizing its average peak area. Further, each compound was determined by its retention time and mass spectrum using Wiley (https://sciencesolutions.wiley.com/solutions/technique/gc-ms/) and National Institute of Standards and Technology (NIST) (https://chemdata.nist.gov/) GC−MS Spectral library.

4.9. Data Collection for ADHD Relevant Genes. Genes associated with ADHD were compiled from two independent, widely used gene-disease association databases, including Gene Cards (https://www.genecards.org/, accessed on March 1, 2024) and DisGeNET (https://www.disgenet.org/search, accessed on March 1, 2024). GeneCards is an integrative database consolidating extensive gene-centric data from over 150 sources, including genomic, clinical, proteomic, genetic, transcriptomic, and functional information. DisGeNET, on the other hand, compiles data from curated databases and scientific literature, offering insights into genes associated with human diseases. To retrieve ADHD-specific genes, we applied a relevance score and a gene-disease association score in both Gene Cards and DisGeNET >0.5, respectively, as described by Ding et al. (2023) and Wang et al. (2022).[46,47] Various key terms related to "ADHD", "attention-deficit/hyperactivity disorder", and "attention deficit disorder" were utilized to search in each database, and gene symbols were collected accordingly. We then integrated and converted the extracted gene symbols from each database into official symbols to eliminate duplicates.

4.10. Functional Interactive Network of ADHD Genes and Mapping Therapeutic Targets. The compiled ADHD genes were subjected to the STRING plug-in Cytoscape (version 3.8.1) to explore their functional interactions at the protein level.[48] In the resulting network, proteins were represented as nodes, and edges depicted their interactions. A default confidence score of ≥0.4 was set to identify potential functional connections, providing a broader understanding of the protein network as represented by Hanes et al. (2023),[49] with a specific focus on "*Homo sapiens*" in Cytoscape. Subsequently, the Cytoscape MCODE plug-in was utilized to dissect the constructed protein network into multiple clusters, highlighting the core functional components with densely interconnected edges.[50] The significant, highly interconnected subnetworks were identified using threshold criteria, including the node score cutoff, degree cutoff, K-core, and max depth parameters. Meanwhile, the established ADHD protein targets were gathered from the Therapeutic Target Database (TTD), accessible at https://idrblab.net/ttd/second March 2024, ChEMBL (https://www.ebi.ac.uk/chembl/, accessed on March 3, 2024), and DrugBank (https://go.drugbank.com/, accessed on March 3, 2024) and mapped with the clusters. These databases provide therapeutic protein target lists, as they offer comprehensive and curated information on experimental and approved drug-target interactions. From the identified clusters, those containing known ADHD protein targets were prioritized to create a focused subnetwork. Further, ShinyGO

https://doi.org/10.1021/acsomega.4c05522
ACS Omega 2025, 10, 4261−4275

available at http://bioinformatics.sdstate.edu/go/ was employed to identify the ontological significance of these selected clusters in a biological system. The CytoHubba plug-in of Cytoscape (version 3.8.1) was utilized to decode the protein with the highest connectivity, and the multiple known protein targets of the subnetwork were selected and designated as a candidate target.[51]

4.11. Ligand Collection and Pharmacokinetic Evaluation. The structures of the identified GC−MS derived compounds were acquired from PubChem in a Spatial Data File (SDF) format. Subsequently, these chemical structures underwent optimization from LigPrep within Maestro, Schrödinger (11.2).[52] Simultaneously, the protein structure of the candidate target was retrieved from the Protein Data Bank (https://www.rcsb.org/). The structure underwent energy minimization by protein preparation wizard Maestro, Schrödinger 11.2 to refine the structure by correcting missing atoms/side chains, optimizing geometry, and assigning protonation states. Employing the OPLS3 force field, atomic positions were adjusted to minimize potential energy, steric clashes, and provide stable, low-energy conformation.[53] Subsequently, the preprocessed protein structure underwent to create a grid box of 10 × 10 × 10 Å dimensions surrounding the active pocket residues. The active pocket residues included in the study were obtained from the PDB. Finally, molecular docking was carried out using the Glide, Maestro, Schrödinger 11.2.[54] The binding affinity of each *H. erinaceus* compound against the candidate target was evaluated by the glide score (kcal/mol).

4.12. Molecular Dynamics of Protein−Ligand Complex. The protein−ligand complex (*H. erinaceus* compound presenting high affinity with the candidate target) underwent MD simulation using Desmond Schrödinger (version 11.2).[55] The simulation setup involved the generation of a widely used default orthorhombic box using the system builder panel for efficient space utilization, flexibility, and maintaining compact protein−ligand complexes.[56] The system was then solvated with a simple point charge or an SPC model. To neutralize the system, an appropriate count of Cl^- or Na^+ ions was added. The simulation duration was set with a trajectory recording interval of 4.8 ps for 100 ns. The ensemble was assigned to NPT conditions, maintaining a 300 K temperature and 1 bar pressure. Then, the simulation interaction diagram panel was utilized to analyze postsimulation parameters, including root-mean-square deviations (RMSD), root-mean-square fluctuations (RMSF), and protein−ligand interaction plots.

4.13. Quantum Mechanical Calculations of the Complex. Hybrid quantum mechanics/molecular mechanics (QM/MM) calculations were conducted utilizing Qsite within Maestro, Schrödinger (Version 11.2) to confirm the bonded interactions between the best binding protein−ligand complex.[57] In this analysis, atoms of the protein residues and ligands involved in binding were designated for the QM region, whereas all of the other atoms were allocated to the MM region. The QM regions were assigned zero charge. The protein−ligand complex underwent full optimization using the B3LYP method for the QM region and the OPLS_2005 force field for the MM region. Default parameters were utilized for other settings. The chemical descriptors, including HOMO denoting highest occupied molecular orbital, LUMO or lowest unoccupied molecular orbital, band gap (ΔE), and molecular electrostatic potential (MESP) were computed. The HOMO and LUMO iso-surfaces of the ligand were generated within the active binding site of the target protein. Additionally, the molecular electrostatic potential surface was analyzed to measure the Poisson−Boltzmann electrostatic potential, with blue colors indicating positive potential regions and red indicating negative potential regions.

5. CONCLUSION

H. erinaceus has gained attention for its traditional medicinal applications, prompting our exploration of its therapeutic potential in ADHD conditions. By integrating ADHD-related genes and constructing protein networks, we identified core proteins in ADHD pathogenesis, highlighting SLC6A4 as a promising therapeutic target. Simultaneously, the *H. erinaceus* aqueous extract revealed a rich phytochemical profile and noncytotoxic effects in SH-SY5Y cell lines. The FTIR unveiled diverse functional groups and further metabolomics analyses through GC−MS provided a variety of compounds. Molecular docking and dynamic simulations pinpointed GC−MS-derived myo-inositol compounds exhibiting potent inhibition against SLC6A4, supported by molecular dynamics and QM/MM analyses demonstrating their structural stability and electron transfer capabilities, respectively. Hence, our findings emphasize the therapeutic promise of myo-inositol compounds of the *H. erinaceus* aqueous extract in ADHD conditions.

■ ASSOCIATED CONTENT

Data Availability Statement

The data sets utilized and analyzed in this study are primarily accessible within the manuscript and supporting files. Additional data can be obtained from the corresponding author upon reasonable request.

Supporting Information

The Supporting Information is available free of charge at https://pubs.acs.org/doi/10.1021/acsomega.4c05522.

Top 10 selected clusters and their ontological significance (PDF)

■ AUTHOR INFORMATION

Corresponding Author

Shiek SSJ Ahmed − *Drug Discovery and Multi-omics Laboratory, Faculty of Allied Health Sciences, Chettinad Hospital and Research Institute, Chettinad Academy of Research and Education, Kelambakkam, Tamil Nadu 603103, India;* orcid.org/0000-0003-3403-4084; Email: shiekssjahmed@gmail.com

Authors

Kamalaharshini Mohan − *Drug Discovery and Multi-omics Laboratory, Faculty of Allied Health Sciences, Chettinad Hospital and Research Institute, Chettinad Academy of Research and Education, Kelambakkam, Tamil Nadu 603103, India*

Nandhakumar Ravichandran − *Drug Discovery and Multi-omics Laboratory, Faculty of Allied Health Sciences, Chettinad Hospital and Research Institute, Chettinad Academy of Research and Education, Kelambakkam, Tamil Nadu 603103, India*

Harish Rajendran − *Drug Discovery and Multi-omics Laboratory, Faculty of Allied Health Sciences, Chettinad Hospital and Research Institute, Chettinad Academy of Research and Education, Kelambakkam, Tamil Nadu 603103, India*

https://doi.org/10.1021/acsomega.4c05522
ACS Omega 2025, 10, 4261−4275

Jency Roshni − *Drug Discovery and Multi-omics Laboratory, Faculty of Allied Health Sciences, Chettinad Hospital and Research Institute, Chettinad Academy of Research and Education, Kelambakkam, Tamil Nadu 603103, India*
Mahema Sivakumar − *Drug Discovery and Multi-omics Laboratory, Faculty of Allied Health Sciences, Chettinad Hospital and Research Institute, Chettinad Academy of Research and Education, Kelambakkam, Tamil Nadu 603103, India*
Janakiraman Velayudam − *Drug Discovery and Multi-omics Laboratory, Faculty of Allied Health Sciences, Chettinad Hospital and Research Institute, Chettinad Academy of Research and Education, Kelambakkam, Tamil Nadu 603103, India*
Sheikh F. Ahmad − *Department of Pharmacology and Toxicology, College of Pharmacy, King Saud University, Riyadh 11451, Saudi Arabia*
Haneen A. Al-Mazroua − *Department of Pharmacology and Toxicology, College of Pharmacy, King Saud University, Riyadh 11451, Saudi Arabia*

Complete contact information is available at: https://pubs.acs.org/10.1021/acsomega.4c05522

Author Contributions

K.M., N.R., and H.R.: writing − original draft, methodology, formal analysis, and data curation; J.R., M.S., and J.V.: writing − editing and formal analysis; S.F.A. and H.A.A.-M: resource and writing − review and editing; S.S.S.J.A.: writing − review and editing, conceptualization, supervision, investigation, and data curation.

Funding

This research was funded by King Saud University, Riyadh, Saudi Arabia, Project Number (RSPD2025R709).

Notes

The authors declare no competing financial interest.

■ ACKNOWLEDGMENTS

All authors thank their institutes for the infrastructure support for this study. The authors acknowledge and extend their appreciation to the Researchers Supporting Project Number (RSPD2025R709), King Saud University, Riyadh, Saudi Arabia, for funding this study.

■ ABBREVIATIONS

ADHD	attention-deficit/hyperactivity disorder
ADRB2	adrenoceptor beta 2
B3LYP Becke	3-parameter, Lee−Yang−Parr
CYP2D6	cytochrome P450 2D6
DA	dopamine
DAT	dopamine transporter
DMEM	Dulbecco's modified Eagle medium
DMSO	dimethylsulfoxide
D-PBS	Dulbecco's phosphate-buffered saline
DPPH	2-diphenyl-1-picrylhydrazyl
DRD1	dopamine receptor D1
ESR1	estrogen receptor alpha
FBS	fetal bovine serum
FTIR	Fourier transform infrared spectroscopy
GC−MS	gas chromatography−mass spectrometry
HE	*Hericium erinaceus*
HOMO	highest occupied molecular orbital
KCNH2	potassium voltage-gated channel subfamily H member 2
LUMO	lowest unoccupied molecular orbital
MAOA	monoamine oxidase A
MAPK	mitogen-activated protein kinases
MESP	Molecular electrostatic potential map
MPH	methylphenidate
MSTFA	*N*-methyl-*N*-(trimethylsilyl)trifluoroacetamide
MTT	(3-(4,5-dimethylthiazol-2-yl)-2,5-diphenyltetrazolium bromide)
NIST	National Institute of Science and Technology
NPT	Isothermal−isobaric
NTRK2	neurotrophic receptor tyrosine kinase 2
OPRM1	opioid receptor mu 1
QM/MM	quantum mechanics/molecular mechanics
RMSD	root-mean-square deviation
RMSF	root-mean-square fluctuations
SERT	serotonin transporter
SLC6A3	solute carrier family 6 member 3
SLC6A4	solute carrier family 6 member 4
TNF	tumor necrosis factor

■ REFERENCES

(1) Fawns, T. Attention deficit and hyperactivity disorder. *Primary Care: Clin. Off. Pract.* **2021**, *48*, 475−491.
(2) Salari, N.; Ghasemi, H.; Abdoli, N.; Rahmani, A.; Shiri, M. H.; Hashemian, A. H.; Akbari, H.; Mohammadi, M. The global prevalence of ADHD in children and adolescents: a systematic review and meta-analysis. *Ital. J. Pediatr.* **2023**, *49*, 48.
(3) Ogundele, M. O. Behavioural and emotional disorders in childhood: A brief overview for paediatricians. *World J. Clin Pediatr.* **2018**, *7*, 9.
(4) Mahone, E. M.; Denckla, M. B. Attention-deficit/hyperactivity disorder: a historical neuropsychological perspective. *J. Int. Neuropsychol. Soc.* **2017**, *23*, 916−929.
(5) Drechsler, R.; Brem, S.; Brandeis, D.; Grünblatt, E.; Berger, G.; Walitza, S. ADHD: Current concepts and treatments in children and adolescents. *Neuropediatrics* **2020**, *51*, 315−335.
(6) Storebø, O. J.; Pedersen, N.; Ramstad, E.; Kielsholm, M. L.; Nielsen, S. S.; Krogh, H. B.; Moreira-Maia, C. R.; Magnusson, F. L.; Holmskov, M.; Gerner, T. et al.Methylphenidate for attention deficit hyperactivity disorder (ADHD) in children and adolescents−assessment of adverse events in non-randomised studies. *Cochrane Database Syst. Rev.* **2018**, .
(7) Naqvi, W.; Singh, A.; Garg, P.; Srivastava, P. Network biology: A promising approach for drug target identification against neurodevelopmental disorders. *Biocell* **2023**, *47*, 1675−1687.
(8) Ekor, M. The growing use of herbal medicines: issues relating to adverse reactions and challenges in monitoring safety. *Front. Pharmacol.* **2014**, *4*, 66193.
(9) Parham, S.; Kharazi, A. Z.; Bakhsheshi-Rad, H. R.; Nur, H.; Ismail, A. F.; Sharif, S.; RamaKrishna, S.; Berto, F. Antioxidant, antimicrobial and antiviral properties of herbal materials. *Antioxidants* **2020**, *9*, 1309.
(10) Modak, M.; Dixit, P.; Londhe, J.; Ghaskadbi, S.; Devasagayam, T. P. A. Indian herbs and herbal drugs used for the treatment of diabetes. *J. Clin Biochem Nutr.* **2007**, *40*, 163−173.
(11) Bell, V.; Silva, C. R. P. G.; Guina, J.; Fernandes, T. H. Mushrooms as future generation healthy foods. *Front. Nutr.* **2022**, *9*, 1050099.
(12) Chong, P. S.; Fung, M.-L.; Wong, K. H.; Lim, L. W. Therapeutic potential of *Hericium erinaceus* for depressive disorder. *Int. J. Mol. Sci.* **2020**, *21*, 163.
(13) Li, I.-C.; Lee, L.-Y.; Tzeng, T.-T.; Chen, W.-P.; Chen, Y.-P.; Shiao, Y.-J.; Chen, C.-C. Neurohealth properties of *Hericium erinaceus* mycelia enriched with erinacines. *Behav. Neurol.* **2018**, *2018*, 5802634.

(14) Baliyan, S.; Mukherjee, R.; Priyadarshini, A.; Vibhuti, A.; Gupta, A.; Pandey, R. P.; Chang, C. M. Determination of antioxidants by DPPH radical scavenging activity and quantitative phytochemical analysis of Ficus religiosa. *Molecules* **2022**, *27*, 1326.
(15) Akash, S.; Aovi, F. I.; Azad, M. A.; Kumer, A.; Chakma, U.; Islam, M. R.; Mukerjee, N.; Rahman, M. M.; Bayıl, I.; Rashid, S.; Sharma, R. A drug design strategy based on molecular docking and molecular dynamics simulations applied to the development of inhibitor against triple-negative breast cancer by Scutellarein derivatives. *PLoS One* **2023**, *18*, No. e0283271.
(16) Javan, M. B.; Soltani, A.; Ghasemi, A. S.; Lemeski, E. T.; Gholami, N.; Balakheyli, H. Ga-doped and antisite double defects enhance the sensitivity of boron nitride nanotubes towards Soman and Chlorosoman. *Appl. Surf. Sci.* **2017**, *411*, 1−10.
(17) Faraone, S. V.; Larsson, H. Genetics of attention deficit hyperactivity disorder. *Mol. Psychiatry* **2019**, *24*, 562−575.
(18) Ginsberg, Y.; Quintero, J.; Anand, E.; Casillas, M.; Upadhyaya, H. P. Underdiagnosis of attention-deficit/hyperactivity disorder in adult patients: a review of the literature. *Prim. Care Companion CNS Disord.* **2014**, *16*, 23591.
(19) Cecil, C. A.; Nigg, J. T. Epigenetics and ADHD: reflections on current knowledge, research priorities and translational potential. *Mol. Diagn. Ther.* **2022**, *26*, 581−606.
(20) Morton, W. A.; Stockton, G. G. Methylphenidate abuse and psychiatric side effects. *Prim Care Companion J. Clin. Psychiatry* **2000**, *2*, 159−164.
(21) Gravina, A. G.; Pellegrino, R.; Auletta, S.; Palladino, G.; Brandimarte, G.; D'Onofrio, R.; Arboretto, G.; Imperio, G.; Ventura, A.; Cipullo, M.; et al. Hericium erinaceus, a medicinal fungus with a centuries-old history: Evidence in gastrointestinal diseases. *World J. Gastroenterol.* **2023**, *29* (20), 3048−3065.
(22) Brandalise, F.; Roda, E.; Ratto, D.; Goppa, L.; Gargano, M. L.; Cirlincione, F.; Priori, E. C.; Venuti, M. T.; Pastorelli, E.; Savino, E.; Rossi, P. Hericium erinaceus in neurodegenerative diseases: From bench to bedside and beyond, how far from the shoreline? *J. Fungi* **2023**, *9*, 551.
(23) Szućko-Kociuba, I.; Trzeciak-Ryczek, A.; Kupnicka, P.; Chlubek, D. Neurotrophic and Neuroprotective Effects of Hericium erinaceus. *Int. J. Mol. Sci.* **2023**, *24*, 15960.
(24) Baishya, T.; Das, P.; Ashraf, G. J.; Dua, T. K.; Paul, P.; Nandi, G.; Jajo, H.; Dutta, A.; Kumar, A.; Bhattacharya, M.; Sahu, R. Antioxidant activity, cytotoxicity assay, and evaluation of bioactive compounds using GC-MS and HPTLC-based bioassay in the extracts of Osbeckia stellata var. crinita (Benth. ex Naudin) grown in Manipur, India. *Kuwait J. Sci.* **2024**, *51*, 100229.
(25) Chen, C.; Wang, J.; Pan, D.; Wang, X.; Xu, Y.; Yan, J.; Wang, L.; Yang, X.; Yang, M.; Liu, G. P. Applications of multi-omics analysis in human diseases. *MedComm* **2023**, *4*, No. e315.
(26) Bollmann, S.; Ghisleni, C.; Poil, S. S.; Martin, E.; Ball, J.; Eich-Höchli, D.; Edden, R. A.; Klaver, P.; Michels, L.; Brandeis, D.; O'Gorman, R. L. Developmental changes in gamma-aminobutyric acid levels in attention-deficit/hyperactivity disorder. *Transl. Psychiatry* **2015**, *5*, No. e589.
(27) Schnorr, I.; Siegl, A.; Luckhardt, S.; et al. Inflammatory biotype of ADHD is linked to chronic stress: a data-driven analysis of the inflammatory proteome. *Transl. Psychiatry* **2024**, *14*, 37.
(28) Becker, S.; Sharma, M. J.; Callahan, B. L. ADHD and Neurodegenerative Disease Risk: A Critical Examination of the Evidence. *Front. Aging Neurosci.* **2022**, *13*, 826213.
(29) Bauer, J.; Werner, A.; Kohl, W.; Kugel, H.; Shushakova, A.; Pedersen, A.; Ohrmann, P. Hyperactivity and impulsivity in adult attention-deficit/hyperactivity disorder is related to glutamatergic dysfunction in the anterior cingulate cortex. *World J. Biol. Psychiatry* **2018**, *19*, 538−546.
(30) Zhong, L.; He, H.; Zhang, J.; Gao, X.; Yin, F.; Zuo, P.; Song, R. Gene Interaction of Dopaminergic Synaptic Pathway Genes in Attention-Deficit Hyperactivity Disorder: a Case-Control Study in Chinese Children. *Mol. Neurobiol.* **2024**, *61*, 42−54.
(31) Pinsonneault, J. K.; Frater, J. T.; Kompa, B.; Mascarenhas, R.; Wang, D.; Sadee, W. Intronic SNP in ESR1 encoding human estrogen receptor alpha is associated with brain ESR1 mRNA isoform expression and behavioral traits. *PLoS One* **2017**, *12*, No. e0179020.
(32) Dean, L.Atomoxetine therapy and CYP2D6 genotype In *Medical Genetics Summaries*, Pratt, V. M.; Scott, S. A.; Pirmohamed, M.; Esquivel, B.; Kattman, B. L.; Malheiro, A. J. Ed.; National Center for Biotechnology Information (US), 2020
(33) Henningsson, S.; Zettergren, A.; Hovey, D.; Jonsson, L.; Svärd, J.; Cortes, D. S.; Melke, J.; Ebner, N. C.; Laukka, P.; Fischer, H.; Westberg, L. Association between polymorphisms in NOS3 and KCNH2 and social memory. *Front. Neurosci.* **2015**, *9*, 393.
(34) Reith, M. E.; Kortagere, S.; Wiers, C. E.; Sun, H.; Kurian, M. A.; Galli, A.; Volkow, N. D.; Lin, Z. The dopamine transporter gene SLC6A3: multidisease risks. *Mol. Psychiatry* **2022**, *27*, 1031−1046.
(35) Carpentier, P. J.; Vasquez, A. A.; Hoogman, M.; Onnink, M.; Kan, C. C.; Kooij, J. J. S.; Makkinje, R.; Iskandar, S.; Kiemeney, L. A.; de Jong, C. A. J.; et al. Shared and unique genetic contributions to attention deficit/hyperactivity disorder and substance use disorders: a pilot study of six candidate genes. *Eur. Neuropsychopharmacol.* **2013**, *23* (6), 448−457.
(36) Kwon, H. J.; Jin, H. J.; Lim, M. H. Association between monoamine oxidase gene polymorphisms and attention deficit hyperactivity disorder in Korean children. *Genet. Test Mol. Biomarkers* **2014**, *18*, 505−509.
(37) Ribasés, M.; Hervás, A.; Ramos-Quiroga, J. A.; Bosch, R.; Bielsa, A.; Gastaminza, X.; Fernández-Anguiano, M.; Nogueira, M.; Gómez-Barros, N.; Valero, S.; et al. Association study of 10 genes encoding neurotrophic factors and their receptors in adult and child attention-deficit/hyperactivity disorder. *Biol. Psychiatry* **2008**, *63* (10), 935−945.
(38) Mariggiò, M. A.; Palumbi, R.; Vinella, A.; Laterza, R.; Petruzzelli, M. G.; Peschechera, A.; Gabellone, A.; Gentile, O.; Vincenti, A.; Margari, L. DRD1 and DRD2 receptor polymorphisms: genetic neuromodulation of the dopaminergic system as a risk factor for ASD, ADHD and ASD/ADHD overlap. *Front. Neurosci.* **2021**, *15*, 705890.
(39) Glessner, J. T.; Khan, M. E.; Chang, X.; Liu, Y.; Otieno, F. G.; Lemma, M.; Slaby, I.; Hain, H.; Mentch, F.; Li, J.; et al. Rare recurrent copy number variations in metabotropic glutamate receptor interacting genes in children with neurodevelopmental disorders. *J. Neurodev Disord.* **2023**, *15* (1), 14.
(40) Mancini, M.; Andreassi, A.; Salvioni, M.; Pelliccione, F.; Mantellassi, G.; Banderali, G. Myoinositol and D-chiro inositol in improving insulin resistance in obese male children: Preliminary data. *Int. J. Endocrinol.* **2016**, *2016*, 8720342.
(41) Kalra, B.; Kalra, S.; Sharma, J. B. The inositols and polycystic ovary syndrome. *Indian J. Endocrinol. Metab.* **2016**, *20*, 720−724.
(42) López-Gambero, A. J.; Sanjuan, C.; Serrano-Castro, P. J.; Suárez, J.; Rodríguez de Fonseca, F. The biomedical uses of inositols: A nutraceutical approach to metabolic dysfunction in aging and neurodegenerative diseases. *Biomedicines* **2020**, *8*, 295.
(43) Lazarova, I.; Nilofar; Caprioli, G.; Piatti, M.; Ricciutelli, M.; Ulusan, M. D.; Koyuncu, I.; Yuksekdag, O.; Mollica, A.; Stefanucci, A.; Zengin, G. Influence of extraction solvents on the chemical constituents and biological activities of Astragalus aduncus from Turkey flora: In vitro and in silico insights. *Arch. Pharm.* **2024**, *357* (9), No. e2400257.
(44) Shaikh, J. R.; Patil, M. Qualitative tests for preliminary phytochemical screening: An overview. *Int. J. Chem. Stud.* **2020**, *8*, 603−608.
(45) Nokhala, A.; Siddiqui, M. J.; Ahmed, Q. U.; Ahamad Bustamam, M. S.; Zakaria. Z.A Investigation of α-glucosidase inhibitory metabolites from Tetracera scandens leaves by GC−MS metabolite profiling and docking studies. *Biomolecules* **2020**, *10*, 287.
(46) Ding, D.; Wang, D.; Qin, Y. Development and validation of multi-omic prognostic signature of anoikis-related genes in liver hepatocellular carcinoma. *Medicine* **2023**, *102*, No. e36190.

https://doi.org/10.1021/acsomega.4c05522
ACS Omega 2025, 10, 4261−4275

(47) Wang, X.; Lu, Y.; Liu, Z.; Zhang, Y.; He, Y.; Sun, C.; Li, L.; Zhai, Q.; Meng, B.; Ren, X.; Wu, X.; Zhang, H.; Wang, X. A 9-LncRNA Signature for Predicting Prognosis and Immune Response in Diffuse Large B-Cell Lymphoma. *Front. Immunol.* **2022**, *13*, 813031.
(48) Doncheva, N. T.; Morris, J. H.; Gorodkin, J.; Jensen, L. J. Cytoscape StringApp: network analysis and visualization of proteomics data. *J. Proteome Res.* **2019**, *18*, 623−632.
(49) Hanes, R.; Zhang, F.; Huang, Z. Protein Interaction Network Analysis to Investigate Stress Response, Virulence, and Antibiotic Resistance Mechanisms in *Listeria monocytogenes*. *Microorganisms* **2023**, *11*, 930.
(50) Bader, G. D.; Hogue, C. W. An automated method for finding molecular complexes in large protein interaction networks. *BMC Bioinf.* **2003**, *4*, 1−27.
(51) Chin, C. H.; Chen, S. H.; Wu, H. H.; Ho, C. W.; Ko, M. T.; Lin, C. Y. cytoHubba: identifying hub objects and sub-networks from complex interactome. *Bmc Syst. Biol.* **2014**, *8*, 1−7.
(52) Sivakumar, M.; Ahmad, S. F.; Emran, T. B.; Angulo-Bejarano, P. I.; Sharma, A.; Ahmed, S. S. Network-Derived Radioresistant Breast Cancer Target with Candidate Inhibitors from Brown Algae: A Sequential Assessment from Target Selection to Quantum Chemical Calculation. *Mar. Drugs* **2023**, *21*, 545.
(53) Sudhan; Janakiraman; Ahmad, S. F.; Wani, A.; Ahmed, S. S. Phytochemicals from Piper betle (L.) as Putative Modulators of a Novel Network-Derived Drug Target for Coronary Artery Disease: An In Silico Study. *Processes* **2023**, *11*, 3064.
(54) Pandi, S.; Kulanthaivel, L.; Subbaraj, G. K.; Rajaram, S.; Subramanian, S. Screening of potential breast cancer inhibitors through molecular docking and molecular dynamics simulation. *BioMed Res. Int.* **2022**, *2022*, 2022.
(55) Janakiraman, V.; Sudhan, M.; Wani, A.; Ahmad, S. F.; Nadeem, A.; Sharma, A.; Ahmed, S. S. J. Pharmacoscreening, molecular dynamics, and quantum mechanics of inermin from Panax ginseng: a crucial molecule inhibiting exosomal protein target associated with coronary artery disease progression. *PeerJ* **2023**, *11*, No. e16481.
(56) Mukhtar, R. M.; Abdelmoniem, N.; Elrufaie, H. A.; Edris, A.; Ghaboosh, H.; Mahgoub, M. A.; Garelnabi, E. A. E.; Osman, W.; Sherif, A. E.; Ashour, A.; Ghazawi, K. F.; Samman, W. A.; Alhaddad, A. A.; Bafail, R.; Ibrahim, S. R. M.; Mohamed, G. A.; Alzain, A. A. Unlocking the potential of approved drugs for the allosteric inhibition of tropomyosin-receptor kinase A using molecular docking and molecular dynamics studies. *Front. Chem.* **2023**, *11*, 1205724.
(57) Cox, P. B.; Gupta, R. Contemporary computational applications and tools in drug discovery. *ACS Med. Chem. Lett.* **2022**, *13*, 1016−1029.

https://doi.org/10.1021/acsomega.4c05522
ACS Omega 2025, 10, 4261−4275